A High-Resolution Climate Model for the U.S. Pacific Northwest: Mesoscale Feedbacks and Local Responses to Climate Change*

ERIC P. SALATHÉ JR.

Climate Impacts Group, Center for Science in the Earth System, University of Washington, Seattle, Washington

RICHARD STEED, CLIFFORD F. MASS, AND PATRICK H. ZAHN

Department of Atmospheric Sciences, University of Washington, Seattle, Washington

(Manuscript received 12 June 2007, in final form 31 March 2008)

ABSTRACT

Simulations of future climate scenarios produced with a high-resolution climate model show markedly different trends in temperature and precipitation over the Pacific Northwest than in the global model in which it is nested, apparently because of mesoscale processes not being resolved at coarse resolution. Present-day (1990–99) and future (2020–29, 2045–54, and 2090–99) conditions are simulated at high resolution (15-km grid spacing) using the fifth-generation Pennsylvania State University–NCAR Mesoscale Model (MM5) system and forced by ECHAM5 global simulations. Simulations use the Intergovernmental Panel on Climate Change (IPCC) Special Report on Emissions Scenarios (SRES) A2 emissions scenario, which assumes a rapid increase in greenhouse gas concentrations. The mesoscale simulations produce regional alterations in snow cover, cloudiness, and circulation patterns associated with interactions between the large-scale climate change and the regional topography and land–water contrasts. These changes substantially alter the temperature and precipitation trends over the region relative to the global model result or statistical downscaling. Warming is significantly amplified through snow–albedo feedback in regions where snow cover is lost. Increased onshore flow in the spring reduces the daytime warming along the coast. Precipitation increases in autumn are amplified over topography because of changes in the large-scale circulation and its interaction with the terrain. The robustness of the modeling results is established through comparisons with the observed and simulated seasonal variability and with statistical downscaling results.

1. Introduction

The Pacific Northwest region of the United States (see map, Fig. 1) is characterized by complex terrain and land–water contrasts, which produce strong spatial gradients in the regional climate and in the atmospheric processes controlling that climate. While global simulations indicate large-scale patterns of change associated with natural and anthropogenic climate forcing, they cannot capture the effects of narrow mountain ranges, complex land–water interactions, or regional variations in land use. A major question in climate science is whether such mesoscale geographical features will significantly alter the local temperature and precipitation trends under climate change. For many resource allocation decisions, information is required at very small scales. For example, Northwest watersheds supplying municipal energy and water are often 50–200 km in horizontal extent with important smaller-scale terrain features. Because global model grids can significantly mischaracterize the topography, land use, and land–water boundaries at this scale, any climate response driven by surface interactions (e.g., snow, orographic effects, vegetation effects) may not be reliable. Therefore, methods for producing climate change scenarios that can fully account for such effects are required.

A number of methods, ranging from statistical downscaling to regional climate models, have been used to apply climate model results to local impacts analyses.

* Joint Institute for the Study of the Atmosphere and Ocean Contribution Number 1404.

Corresponding author address: Eric P. Salathé Jr., Climate Impacts Group, Center for Science in the Earth System, University of Washington, Box 354235, Seattle, WA 98195-4235.
E-mail: salathe@washington.edu

DOI: 10.1175/2008JCLI2090.1

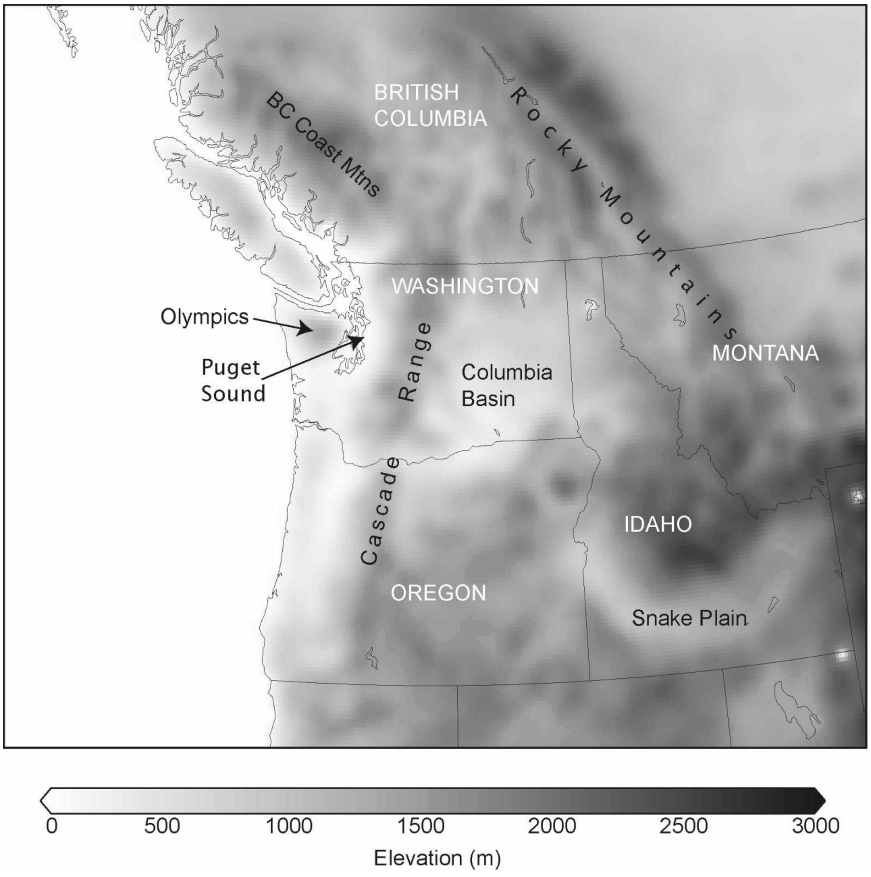

FIG. 1. Geography and topography of the Pacific Northwest.

While statistical methods have been successfully employed in the Pacific Northwest (Salathé, 2003, 2005; Widmann et al. 2003; Wood et al. 2004) and other regions (Giorgi and Mearns 1999), they generally cannot capture the changes in the local climate that result from interactions and feedback between the large-scale atmospheric state and mesoscale processes. Regional climate models attempt to simulate such interactions. Until recently, however, such models have not been run at sufficiently fine grid spacing to properly resolve these mechanisms. For example, Wood et al. (2004) compared the results of a climate change simulation downscaled to the Pacific Northwest using a regional climate model run at 0.5° (~50 km) grid spacing and downscaled to 0.125° spacing using a statistical method that preserves the trend in the global model. The regional model and statistical method both produced a uniform warming trend across the region, with differences of less than a degree Celsius between the two methods. In another study, Duffy et al. (2006) used four regional models, run at 36- to 60-km grid spacing, to simulate climate change over California. The simulations provided little evidence for a substantially different trend in warming in the regional models compared to the global model providing the boundary conditions.

High spatial resolution is essential to simulate mesoscale processes and their interactions with the large-scale forcing. Without properly resolving these processes, a regional climate model is unlikely to improve on results from statistical downscaling. The effect of horizontal resolution on regional climate and weather simulations has been discussed extensively in the literature (Achberger et al. 2003; Christensen and Kuhry 2000; Colle et al. 1999; Colle et al. 2000; Duffy et al. 2003; Leung and Qian 2003; Mass et al. 2002). Studies of 2 yr of fifth-generation Pennsylvania State University (PSU)–National Center for Atmospheric Research (NCAR) Mesoscale Model (MM5) weather forecasts for the Pacific Northwest (Colle et al. 2000; Mass et al. 2002) show clear improvements between 36- and 12-km grid spacing for precipitation, 10-m wind, 2-m temperature, and sea level pressure. Further increasing the resolution to 4 km provides more detail and structure (e.g., defining steeper orographic slopes) but had only a limited impact on forecast skill, possibly resulting from limitations of current verification approaches. To ex-

plore model resolution, Leung and Qian (2003) performed a 5-yr simulation using National Centers for Environmental Prediction (NCAR)–NCEP reanalyses to provide boundary conditions for simulations on 40- and 13-km two-way nested grids. They found that, compared to the 40-km nest, the higher-resolution nest yields more realistic precipitation patterns and produces more frequent heavy precipitation, which is consistent with observations. To understand the effects of climate change on regions like the Pacific Northwest, resolving mesoscale processes controlling precipitation, temperature, and winds is critical. Previous studies over the region (Mass et al. 2003) indicate that grid spacing of 15 km or finer is necessary.

To achieve long regional climate model simulations, several issues must be considered that do not arise in short-term weather forecasting. Interactions between the atmosphere and land surface are critical to the mesoscale climate response, and we have implemented a parameterization to allow the deep soil temperature to interact with the surface changes rather than use a prescribed value. Another important innovation in this study is the use of grid nudging in the outermost nest of the mesoscale model forced by the global model. This technique applies the large-scale forcing to the outermost nest of the mesoscale model across the entire domain in order to preserve the large-scale state from the global model and to ensure mass conservation.

In this paper, we present a regional climate model developed for the U.S. Pacific Northwest and run at high spatial resolution (15-km grid spacing) with global climate model fields used for boundary conditions. This regional model is based on MM5 and uses a configuration similar to that used for operational weather forecasting over the region (Mass et al. 2003). We describe simulations forced by ECHAM5 global simulations of present-day (1990–99) and future (2020–29, 2045–54, and 2090–99) conditions. These simulations illustrate a number of mesoscale effects that produce markedly different climate responses in the mesoscale model compared to the parent global model used to force the regional simulations. In particular, we find localized amplification of wintertime warming and intensification of autumn precipitation in the mesoscale model relative to the global model. These results are then related to mesoscale processes and feedbacks simulated by the regional model.

2. Model setup

To model the regional climate, we employ a limited-area atmospheric model, MM5, with boundary conditions prescribed by simulations from the ECHAM5/Max Planck Institute Ocean Model (MPI-OM) coupled atmosphere–ocean climate model.

a. Forcing data

The atmospheric component of ECHAM5/MPI-OM is the fifth-generation general circulation model developed at the European Centre for Medium-Range Weather Forecasts and the Max Planck Institute for Meteorology (Roeckner et al. 1999, 2003), and the ocean component is the MPI-OM (Marsland et al. 2003). Here we will refer to the coupled model simply as ECHAM5. The global simulation used in this study was performed for the Intergovernmental Panel on Climate Change (IPCC) Fourth Assessment Report (AR4) and was forced with the Special Report on Emissions Scenarios (SRES) A2 emissions scenario (Nakicenovic and Swart 2000). The A2 scenario entails a relatively aggressive increase in atmospheric carbon dioxide emissions over the twenty-first century. ECHAM5 was run at T63 spectral resolution, which corresponds to a horizontal grid spacing of approximately 140 km $\times$ 210 km at midlatitudes, and 32 levels in the vertical. Model output at 6-hourly intervals was obtained from the Climate and Environmental Retrieval and Archive (CERA; information available online at http://cera-www.dkrz.de/CERA/index.html), and the data are managed by World Data Center of Climate (online at http://www.mad.zmaw.de/wdcc/).

The ECHAM5 model results were compared with other models participating in the IPCC AR4 to assess its performance in simulating twentieth-century climate and its projected change in temperature and precipitation for the U.S. Pacific Northwest region (Salathé et al. 2007). While the ECHAM5 simulations shows biases in temperature and precipitation typical of global models, the annual cycle of both is well reproduced. Furthermore, given its relatively high horizontal and vertical resolution, this model produces realistic synoptic-scale patterns over the eastern Pacific and western North America.

We also present regional simulations forced by reanalysis fields in order to isolate deficiencies in the regional model without the complexity of biases inherited from the forcing model. Specifically, we use the NCEP–NCAR Reanalysis Project (NNRP) fields (Kalnay et al. 1996) for the 10-yr period of 1990–99. Data are available at 6-hourly intervals, 2.5° $\times$ 2.5° horizontal grid spacing (approximately 275 km $\times$ 200 km), and 17 pressure levels in the vertical.

b. Regional model

MM5 release 3.6.3 was used as the regional climate model. MM5 was developed for mesoscale weather

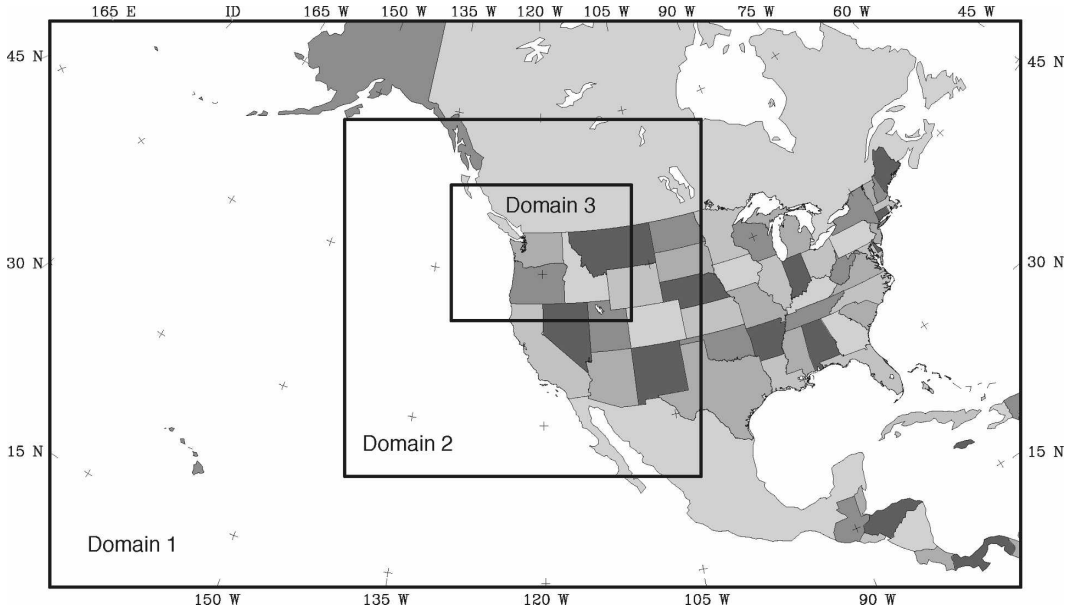

FIG. 2. Mesoscale model domains for the current study. Grid spacing: domain 1, 135 km; domain 2, 45 km; domain 3, 15 km.

forecasting and has been operating in real time at the University of Washington (Mass et al. 2003), and many other places, for over a decade (Mass and Kuo 1998); more recently, it has been used as a tool for regional climate modeling (e.g., Leung and Qian 2003). MM5 is a limited-area, nonhydrostatic, terrain-following sigma-coordinate model (Grell et al. 1993). Parameterizations include the Kain–Fritsch convective parameterization (Kain and Fritsch 1993), the Medium-Range Forecast model (MRF) planetary boundary layer (PBL) scheme (Hong and Pan 1996), the Community Climate Model version 2 (CCM2) radiation scheme (Hack et al. 1993), and the simple ice cloud microphysics (Dudhia 1989).

High regional model resolution is achieved by using multiple MM5 nests at 135-, 45-, and 15-km horizontal grid spacing. Figure 2 shows the MM5 nests used in this study. One-way nesting is utilized. To capture the large-scale processes important for Pacific Northwest climate, the outermost MM5 domain encompasses nearly the entire North American continent and much of the eastern Pacific Ocean. The use of such a large outer domain keeps the outer mesoscale boundaries far from the region of study and ensures that weather systems approaching the Pacific Northwest are well represented by the time they reach the region. The second nest covers the western United States and portions of Canada and Mexico, capturing storm systems and Southwest monsoon circulations that influence the Pacific Northwest. The innermost domain covers the states of Washington, Oregon, and Idaho and the entire Columbia River basin.

Particularly over large domains, the regional model solution can drift over time from that of the driving global climate model. If we assume that the global climate model reasonably captures synoptic-scale structures and that the goal of the dynamic downscaling system is simply to obtain finescale detail for a given large-scale pattern, then the regional model should not modify the large-scale patterns, and such drift is undesirable. This issue has been addressed in the MM5-based real-time numerical weather forecasting system used at the University of Washington (Mass et al. 2003), and nudging is applied to the outermost model domain using the forcing fields of the parent model. We follow the same approach for the climate simulations, with the ECHAM5 forcing fields used for nudging. When nudging is applied in MM5, Newtonian relaxation terms are added to the prognostic equations for wind, temperature, and water vapor to relax the simulation toward the forcing model. The relaxation takes place throughout the interior of the domain and at all vertical levels above the planetary boundary layer. The inner two domains are not nudged, allowing the mesoscale model to freely develop atmospheric structures at finer spatial scale. Results from the real-time forecast system and von Storch et al. (2000) show that nudging is able to keep simulated states close to the driving state at large scales while still generating small-scale features. Thus, this approach maintains the objective of downscaling, which is to generate mesoscale meteorological details consistent with the large-scale state simulated by the global model.

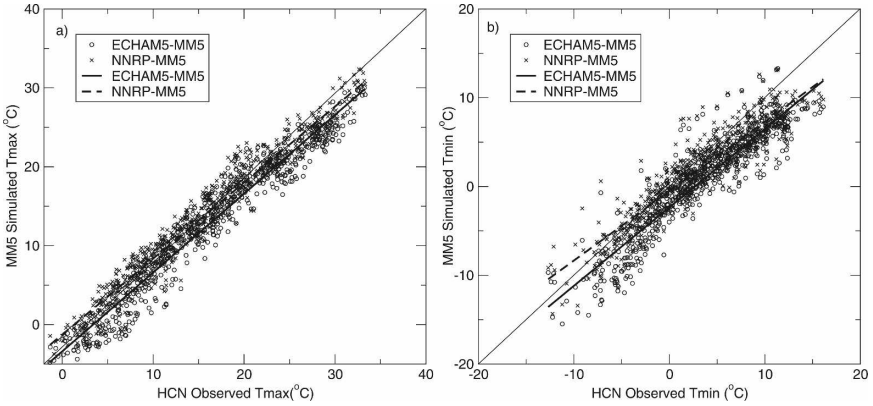

FIG. 3. Scatterplot of observed and simulated 10-yr monthly mean (a) daily maximum temperature and (b) daily minimum temperature for 55 stations in the MM5 simulation domain.

Accurate representation of land–atmosphere interactions in climate models is critical to the realistic simulation of surface energy and water cycles (Wang et al. 2004), which directly influence air temperature, air moisture, and snow dynamics. Snowpack is particularly critical in regions such as the Pacific Northwest where snowmelt plays a central role in regional hydrology. To capture these processes in the climate system over decades, the soil column must freely interact with the atmosphere. In the Noah land surface model (LSM), however, the 3-m-deep soil temperature is prescribed as a constant climatological value, which does not allow the soil column to realistically respond to climate forcing. We have thus implemented a simple method to update the lower boundary soil temperature during the simulation as described in the appendix. This method, tested over extended contemporary periods, provides realistic evolving deep soil temperatures on the mesoscale.

Regional model runs were completed for the following four decades: 1990–99, 2020–29, 2045–54, and 2090–99. Ten-year time slices were chosen in order to strike a balance between a long enough time period to sample interannual variability, such as ENSO variability, but short enough to isolate a time period for which global climate change would essentially be static. The CO_2 concentration was held constant in MM5 for each 10-yr simulation and set to the average value for the decade according to the SRES A2 emissions scenario. Specifically, we have used 361 ppmv for 1990–99, 434 ppmv for 2020–29, 532 ppmv for 2045–54, and 813 ppmv for 2090–99.

3. Model evaluation

To evaluate the regional model performance, we present results from two 10-yr simulations of the current climate (from September 1989 to August 1999). The first simulation is forced by the NCEP–NCAR reanalysis (NNRP–MM5) and the second is forced by the ECHAM5 global climate model (ECHAM5–MM5). The regional model (MM5) is the same for both cases. Each simulation starts after a 1-yr spinup that is not used in the analysis. Because the reanalysis is driven by observations and simulates the large-scale historical daily weather, the NNRP–MM5 simulation represents an idealized case where we can assume that minimal bias either is introduced from the global forcing fields or is due to interannual variability. Discrepancies between the regional simulation and observations would primarily reflect deficiencies in the regional model, for example, resulting from deficient model physics. For the ECHAM5–MM5 simulation, large-scale biases in the global simulation are potentially introduced, although this model performs relatively well for the Pacific Northwest region compared to other global models (Salathé et al. 2007).

Model evaluation is performed at the station level and includes verification across the seasonal cycle. Here we present results for 55 stations across Washington, Oregon, and Idaho. These stations are selected from the Historical Climate Network (HCN; Karl et al. 1990) such that all are at elevations within 500 ft of the collocated MM5 grid cell.

a. Temperature

The 10-yr monthly average daily maximum temperature (Tmax) and minimum temperature (Tmin) were obtained for the HCN observations and the ECHAM5–MM5 and NNRP–MM5 simulations at each station location and for each calendar month. To summarize all stations and months, Fig. 3 shows scatterplots of observed and simulated Tmax (Fig. 3a) and Tmin (Fig. 3b)

TABLE 1. Regression analysis for station results.

	Correlation	Slope	Bias
NNRP–MM5 Tmax	0.98	0.96	−1.86°C
ECHAM5–MM5 Tmax	0.97	1.00	−3.41°C
NNRP–MM5 Tmin	0.92	0.78	−1.25°C
ECHAM5–MM5 Tmin	0.93	0.88	−2.73°C
ECHAM5–MM5 Pcp*	0.91	0.89	0.069 mm day^{-1}
NNRP–MM5 Pcp	0.92	0.95	0.076 mm day^{-1}

* Pcp ≡ precipitation.

for each monthly value from each station; results for the ECHAM5–MM5 and NNRP–MM5 simulations are indicated by black dots and open circles, respectively. Results of regression analysis of the station data are presented in Table 1. For both simulations, Tmax shows a much better correlation and regression coefficient (slope) than Tmin, but Tmin produces a slightly smaller overall bias. The ECHAM5–MM5 simulation has a larger cold bias in both Tmax and Tmin than the NNRP–MM5 simulation, reflecting the additional bias introduced by the free-running climate model relative to reanalysis data. The cold bias in the ECHAM5–MM5 Tmin simulation increases as observed temperature falls below 0°C, which is not seen in the NNRP–MM5 simulation, suggesting that the ECHAM5 model introduces a cold bias in winter.

The low slope for Tmin indicates an increasing cold bias in Tmin in warmer months and locations, which is evident in Fig. 3b as the simulated values fall below the 1:1 line above 5°C. In fact, for ECHAM5–MM5, the relationship between the observed and simulated Tmin is not linear, with a small bias around 0°–5°C and a larger bias at both warmer and cooler temperatures. To explore the seasonal aspect of this behavior, we average the temperature bias over all stations for each calendar month for Tmax and Tmin (Fig. 4). For the NNRP–MM5 simulation, the bias in Tmax is relatively constant over the year, fluctuating around the mean of −1.9°C. The Tmin, however, shows a strong seasonality, with little bias in winter months and a considerable bias in summer that exceeds the bias in Tmax. The results for the ECHAM5–MM5 simulation are more complex because of the additional bias inherited from the global model. The cold bias in ECHAM5 is partly due to synoptic-scale cold outbreaks in winter, which are not found in the reanalysis. The cold outbreaks appear to be related to inadequate blocking of continental air masses by the Rocky Mountains, which are weakly resolved in the climate model.

b. Precipitation

Figure 5 shows the observed and simulated precipitation for all stations and months, and results of the linear regression are shown in Table 1. Despite considerable scatter compared to the temperature simulation, there is strong correlation, better than 90%, between observations and both simulations. An overall wet bias is evident, and appears to be greatest for the months and stations of moderate precipitation. The seasonal characteristic of this bias is illustrated in Fig. 6, which shows the difference between the observed and simulated precipitation averaged over all stations for each month. For summer months, there is a small dry bias in both simulations, with the low bias in the NNRP–MM5

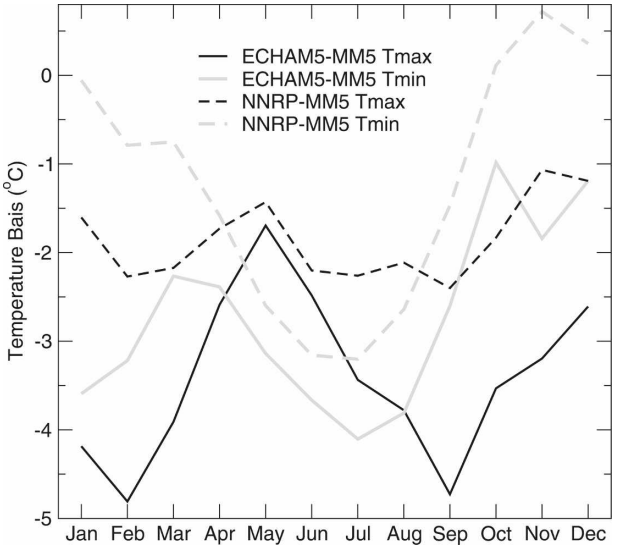

FIG. 4. Annual cycle of bias between observed and simulated temperatures averaged over all 55 stations.

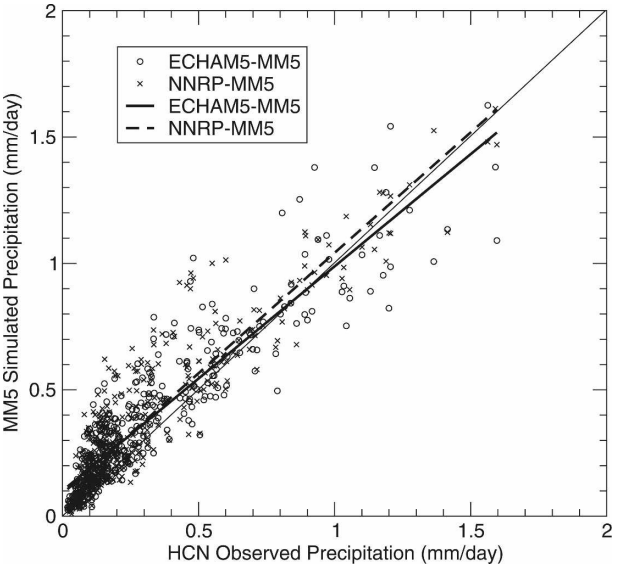

FIG. 5. Scatterplot of observed and simulated precipitation for 55 stations in the MM5 simulation domain.

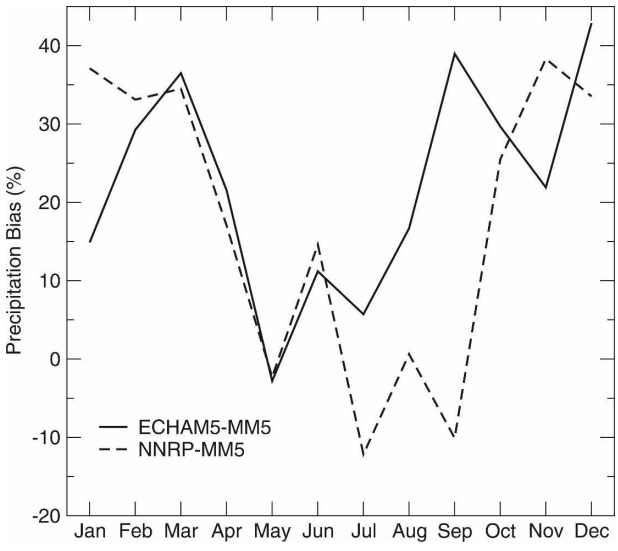

FIG. 6. Annual cycle of bias between observed and simulated precipitation, expressed as a percent of the observed precipitation, and averaged over all 55 stations

simulation extending into September. For winter months, there is a substantial wet bias, resulting from the excess precipitation simulated for dry stations. Because the bias is expressed as a percent of the station mean, the wet bias at dry stations contributes substantially to the domain-averaged bias despite accounting for a small amount of the domain total precipitation.

4. Results

Below we present the overall features and patterns of change in the ECHAM5–MM5 climate change simulations relative to the base climate. Because of the large interannual climate variability in the Pacific Northwest, it is difficult to establish robust trends from the four 10-yr time slices. However, many features appear to be related to known large-scale forcings and physical processes. In this section, we will examine how the MM5 simulation differs from the global ECHAM5 model. In following section, we shall discuss in more detail the physical mechanisms responsible for these results.

a. Temperature

Figures 7a–c show the change in winter [December–February (DJF)] 2-m air temperature from the regional model. Differences are between the current climate (1990–99) and the three future decades of 2020–29 (Fig. 7a), 2045–54 (Fig. 7b), and 2090–99 (Fig. 7c). A distinct geographic pattern develops over time. In addition to domain-wide warming, the model produces amplified warming along the flanks of the mountain ranges and across the high plains of eastern Washington, eastern Oregon, and southern Idaho. This pattern is well established in the 2020s and becomes stronger through the simulation, yielding considerable localized warming by the 2090s. The dominant features of the warming pattern remain the same in each simulated decade as the warming intensifies. This result suggests that the pattern is not overly affected by interannual variability, but is controlled by interactions between the large-scale forcing from the ECHAM5 model with the regional terrain and land–water contrasts.

For the other seasons of the year, the warming patterns are again similar for each decade, so only the 2045–54 results are shown in Figs. 7d–f. For March–May (MAM; Fig. 7d), we again find amplified warming following the terrain. In this case, however, the amplification is at the highest elevations, following the crest of the Cascade Range. A considerably lower warming rate is simulated along the coast, west of the Cascade Range. For June–August (JJA; Fig. 7e) and September–November (SON; Fig. 7f), the regional model does not produce significant finescale features in the simulated warming. An exception is the large warming rates for the high elevations of the British Columbia, Canada, Coast Mountains for JJA.

b. Precipitation

Figure 8 shows the change in annual average precipitation (mm day^{-1}) from 1990–99 to the three future 10-yr simulations (positive values indicate increased precipitation in the future decade). The mesoscale simulations performed here show no persistent trend in the annual total precipitation pattern over the three decades. There is some similarity in the patterns for 2020–29 (Fig. 8a) and 2045–54 (Fig. 8b), with decreases over southwestern British Columbia and increases over the northern Cascades and Rockies. However, a very different pattern is simulated for the 2090s (Fig. 8c), with large decreases along the mountains of Oregon and south/central Washington and increases along the mainland British Columbia coast. While there is considerable variability in the response over coastal and mountain regions, a modest increase in precipitation is consistently found over the inland portion of the domain. The precipitation change for the 2045–54 simulation is broken down by season in Fig. 9. While DJF shows a decrease in precipitation over the northwest part of the domain, widespread increases are simulated for MAM (the northern Cascades and coastal British Columbia) and SON (Cascades of Washington and Oregon). The consensus of the multimodel ensemble used in the IPCC AR4 indicates a modest positive trend over

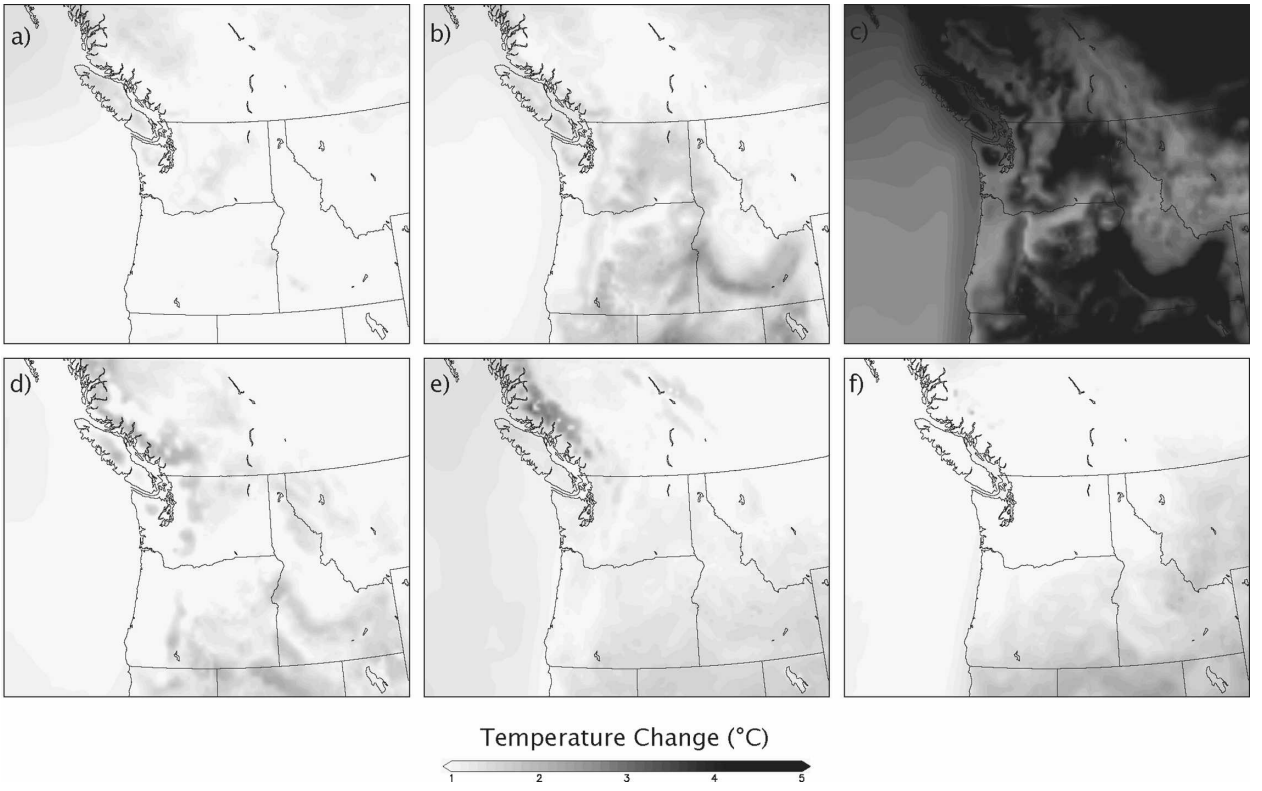

FIG. 7. Simulated seasonal temperature changes (°C) relative to 1989–99 for (a) DJF 2020–29, (b) DJF 2045–55, (c) DJF 2090–99, (d) MAM 2045–55, (e) JJA 2045–55, and (f) JJA 2045–55.

the region (Christensen et al. 2007) and a statistically significant increase in extreme precipitation (Tebaldi et al. 2006). The most striking patterns of change seen in Fig. 9 are related to mesoscale interactions with the surface that are not captured in global models. These mesoscale features will be the focus of the discussion below, and not the overall trends, which are not well characterized by these experiments.

5. Regional effects on temperature

a. Snow–albedo feedback

Snow–albedo feedback plays a pivotal role in global climate model simulations (Holland and Bitz 2003). Global models, however, cannot realistically represent this feedback at regional scales because they do not resolve the slopes and elevations of the regional topography or the mesoscale distribution of snow. Previous research with regional models has shown that this feedback may operate at fine spatial scales. Giorgi et al. (1997) report amplified warming with elevation both in observations and in a regional climate model for the Alpine region. Leung and Ghan (1999) show amplified warming in MM5-based simulations for the Pacific Northwest. Duffy et al. (2006) compare snow albedo effects in simulations from several regional models over southwestern North America. Amplified warming is seen along the Sierra Nevada Mountains in results from an MM5-based run at 50-km grid spacing. Three other models were included in this study, the Mesoscale Atmospheric Simulation (MAS) model at 36-km grid spacing, the Regional Spectral Model (RSM) at 60-km grid spacing, and the Second-Generation Regional Climate Model (RegCM2) at 52-km grid spacing. These models do not show a comparable effect to MM5; however, these are spectral models, which have difficulty adequately representing the topography at this grid spacing.

For the simulations at 15-km resolution presented here, the snow–albedo feedback yields considerable finescale spatial structure. Regions of amplified warming, following the terrain, are evident in the regional simulations for DJF (Figs. 7a–c) and MAM (Fig. 7d). Figure 10a shows the DJF temperature change from 1990–99 to 2045–54 in the ECHAM5–MM5 regional simulation minus the temperature change in the global ECHAM5 model over the same period. Positive values (red) indicate more warming in the regional model than the raw global model; negative values (blue) indicate less warming. For the highest elevations in the Rockies

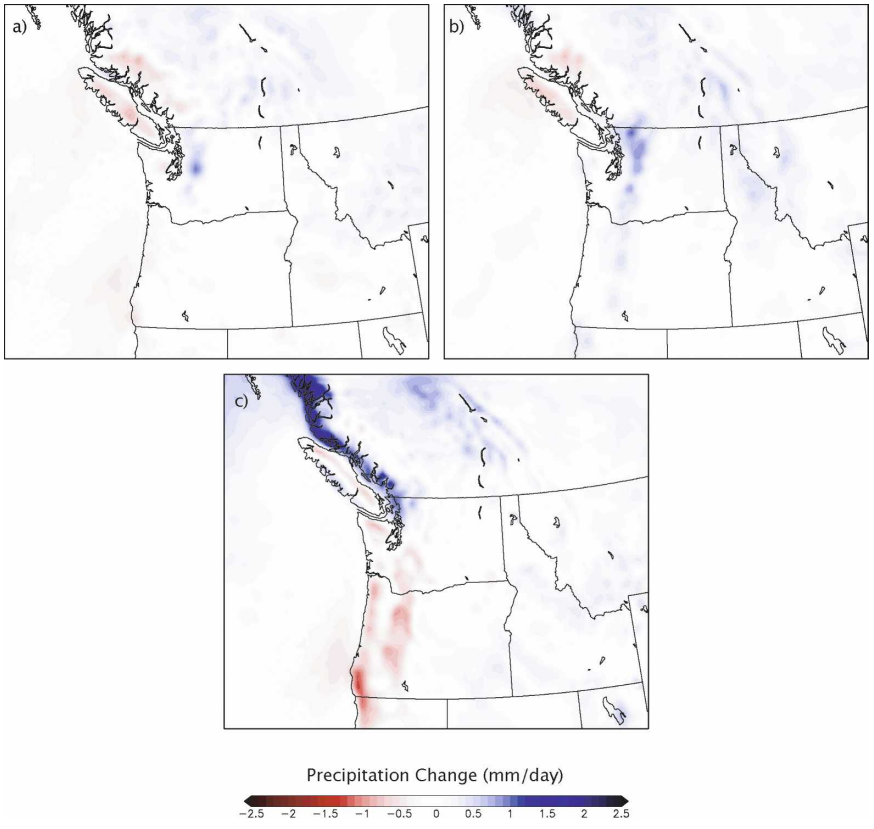

FIG. 8. Simulated annual mean precipitation changes (mm day^{-1}) relative to 1990–99 for (a) 2020–29, (b) 2045–55, and (c) 2090–99.

and for British Columbia, the regional model shows less warming than the global model; reasons for this behavior are discussed below. Over the remainder of the domain, the regional model produces considerably more warming than the global model. This amplified warming occurs along the flanks of the Cascade Range and over high basins. These areas are at the margins of the snowpack in the present climate and where the snowpack is most sensitive to warming temperatures. Figure 10b shows the DJF season snow loss from 1990–99 to 2045–54 as indicated by the reduced frequency of days with more than 50% snow cover. Figure 10c shows the change in albedo over the same period. The warming pattern clearly matches the loss in snow and the decreased albedo. Local amplification of warming in the mesoscale model relative to the raw global model exceeds 1°C over much of eastern Washington and Oregon and 2°C over the Snake River plain in southern Idaho for the 2040s.

The regions with larger warming in the global model than in the regional model (blue areas in Fig. 10a) result in part from the inability of the global model to properly resolve the snow–albedo feedback. Figure 11 shows the warming in the ECHAM5 model from 1990–99 to 2045–54, with contour lines indicating the topographic relief for the model. The region of the greatest warming lies along the western slopes of the Rocky Mountains, as depicted by the model topography. This area corresponds to the margins of the snowpack in the model, which yields a large reduction in surface albedo resulting from snow loss (not shown) in the climate change simulation. The topography in the ECHAM5 model, however, is substantially different from the true topography, and the region represented as having high elevations in British Columbia, Canada, is in fact a low basin between the Rocky Mountains and Coast Range (Fig. 1), which has considerably different sensitivity to snow cover. Thus, the amplified warming depicted in the raw ECHAM5 model over these regions is spurious, and leads to the larger warming trend in these locations relative to the regional model.

b. Validation of simulated snow–albedo feedback

Confidence in the simulated snow–albedo feedback depends on the following two conditions: 1) the present-day snow cover must be reasonably captured

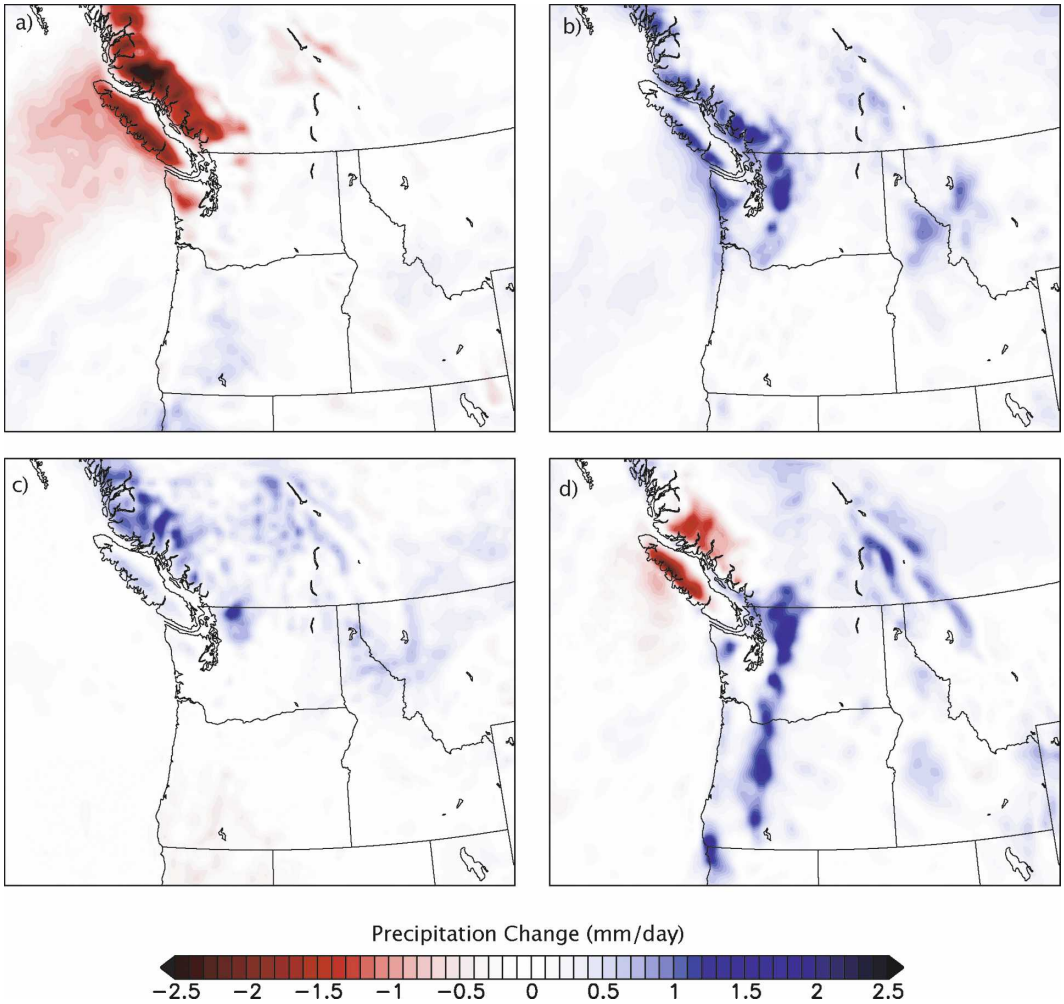

FIG. 9. Simulated seasonal precipitation changes (mm day^{-1}) from 1989–99 to 2045–55 from the ECHAM5–MM5 regional model for (a) DJF, (b) MAM, (c) JJA, and (d) SON.

by the model because the feedback will occur at the margins of the snow-covered area, and 2) the change in snow cover and albedo for a given amount of warming must be reasonably captured in order to represent the magnitude of the feedback. Given the mixed results in the literature and uncertainty in the difficulty in validating present-day snow cover, we shall evaluate the snow–albedo feedback in the model by comparing the transition from winter to spring as simulated by the model and as captured by station observations.

The transition from winter to spring in the Pacific Northwest produces a significant retreat of the snow line along the slopes of major mountain ranges and in elevated basins. We shall use this change as an analog for climate change to test the model. The difference between the April and January 10-yr monthly mean surface (2 m) air temperature for the 1990–99 ECHAM5–MM5 simulation is shown in Fig. 12a, and indicates a similar spatial pattern to the climate change pattern shown in Fig. 7. To illustrate the role of snow cover in this seasonal change pattern, we compute, at each grid cell, the fraction of days in the decade with 50% or greater snow cover for each calendar month. Figure 12b shows the change in the fractional snow cover from January to April from the 1990–99 simulation. There is intensified warming at the locations of maximum loss of snow cover, indicating that MM5 simulates a snow–albedo interaction in the transition from January to April, and this effect helps determine the spatial pattern of warming.

To verify this seasonal warming pattern, we may compare the regional simulation to station observations. The U.S. HCN (information available online at http://www.ncdc.noaa.gov/oa/climate/research/ushcn/ushcn.html; see also Karl et al. 1990) includes 113 observing stations in Washington, Oregon, and Idaho with

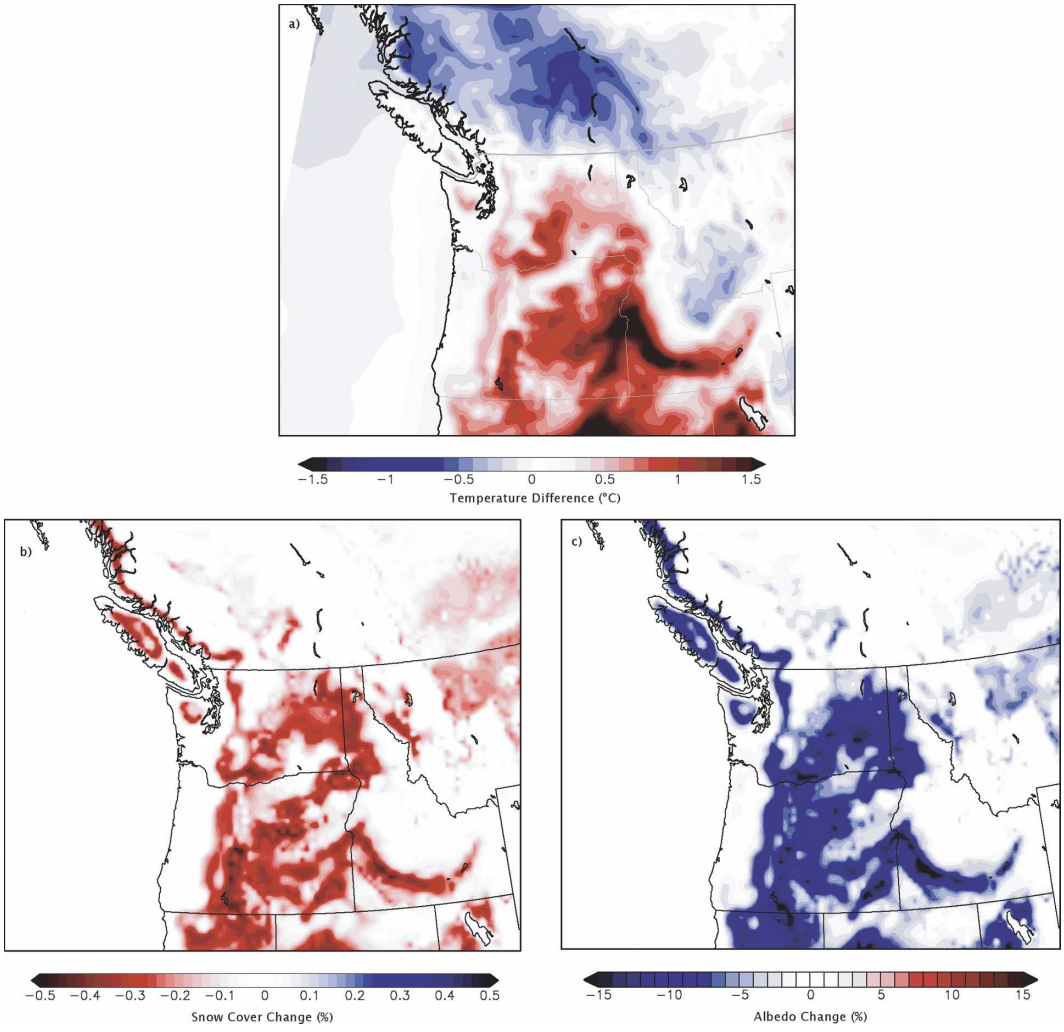

FIG. 10. Changes from 1990s to 2050s December–February season for (a) difference in raw model change and mesoscale model change in 2-m air temperature, (b) frequency of 50% snow cover, and (c) surface albedo.

good coverage of the patterns of warming and snow loss depicted in Fig. 12. We compute the 10-yr mean (1990–99) January–April temperature change at each station and, in Fig. 13, plot this value against the corresponding grid cell value from the MM5 simulation. The model produces a small overestimate of the seasonal warming, but this bias is uniform across all stations, and thus is not related to snow processes. Importantly, the contrast between regions of strong and weak warming corresponds quite well between the model and station network, as indicated by the slope of 0.91 and correlation of 0.82, suggesting that the model does not exaggerate warming in areas where there is snow cover in January.

Reproducing the pattern of seasonal change tests many basic elements of the climate system response associated with snow cover. Success in capturing the seasonal warming pattern suggests that the model correctly captures the interactions between snow and warming in the seasonal cycle. Certainly, if a model cannot capture this seasonal pattern of change, one cannot have confidence in the simulated patterns associated with climate change. Furthermore, these observed changes occur on a spatial scale that cannot be depicted in a global model or coarse-resolution regional model.

c. *Spring cloudiness and diurnal temperature in spring*

For the spring season (March–May), the enhanced warming seen for winter moves upslope following the snow line, and maximum warming is found along the crest of the Cascade Range and the Rockies north of the Snake Plain. In addition, the regional model reveals a complex response in the diurnal temperature range.

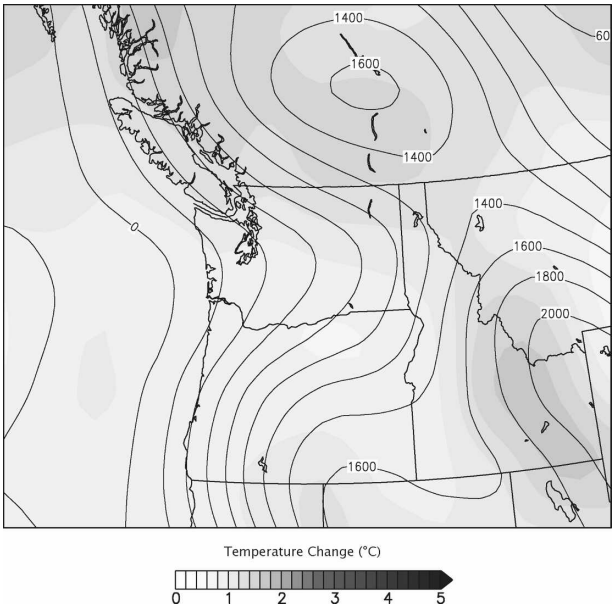

FIG. 11. Change from 1990s to 2050s in 2-m air temperature (°C) in raw ECHAM5 model. Contours indicate model terrain height (m).

Figure 14 shows the difference in simulated MAM warming from 1989–99 to 2045–54 between the ECHAM5 global simulation and the ECHAM5–MM5 regional simulation for Tmax (Fig. 14a) and Tmin (Fig. 14b). Positive values indicate larger warming in the regional simulation. Along the coastal zone west of the Cascades, the regional model shows considerably less warming of maximum daytime temperatures than the raw ECHAM5 model. In the mountains, where snow–albedo feedback is important, the warming is greater for the regional simulation. Nighttime minimum temperatures show greater warming in the regional model than the global model for most of the domain, including the regions that show less warming during daytime.

The greater warming of the continental interior, relative to the oceans, establishes an anomalous onshore pressure gradient, as seen from the 850-hPa height field (change from the 1990s to the 2050s, see Fig. 14c). This pressure gradient increases the climatological onshore flow (streamlines in Fig. 14d) and low-level cloudiness as indicated by the change in integrated surface to 850-hPa cloud water concentration (Fig. 14d). Clouds increase over the coastal ocean and inland along the windward slopes of the terrain, suggesting increased clouds banked against the coastal mountains. The increase in low-level cloudiness is derived from two effects. The ECHAM5 global simulation and the 45-km regional domain (not shown) indicate an overall increase in maritime clouds off the U.S. West Coast associated with a strengthening of the east Pacific high. The high shifts eastward in each of the ECHAM5–MM5 future simulations (i.e., 2020–29, 2045–54, 2090–99) relative to the base climate (1990–99). Thus, the increase in regional cloudiness is due both to the large-scale increase in maritime cloudiness under the Pacific high, which is inherited from the ECHAM5 forcing fields, and the anomalous onshore winds, which is due to mesoscale land–sea effects.

The mechanism for the changes in the Pacific high is not clear, and this result is not seen in all global models

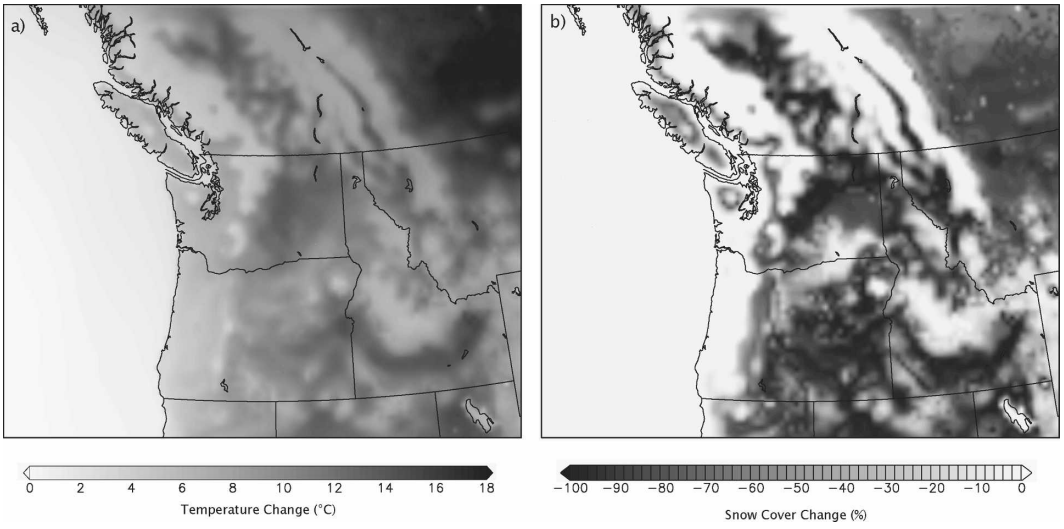

FIG. 12. April − January 1990s ECHAM5–MM5 simulation (a) 2-m air temperature and (b) fraction of days with 50% snow cover of grid cell.

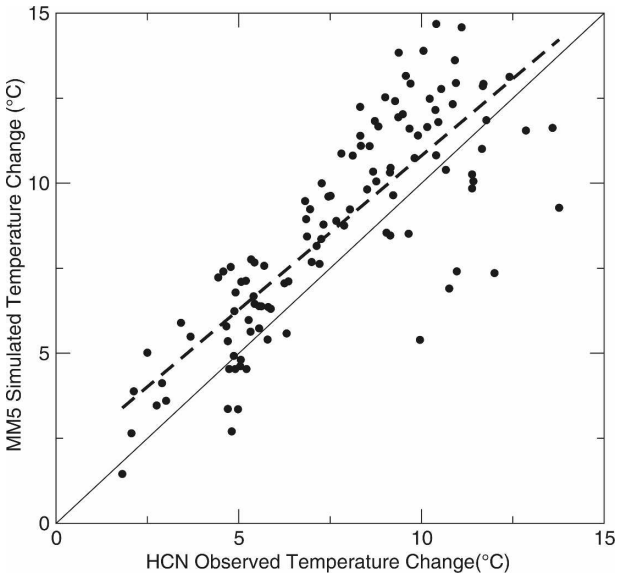

FIG. 13. Comparison of observed (HCN) and simulated (MM5) change in air temperature from January to April.

(Croke et al. 1999). Therefore, to the extent that these results for increased cloudiness depend on changes in the Pacific high, they would not be consistently reproduced using other global models to force the regional simulation. Nevertheless, observational studies have shown increased cloudiness over the coastal Southwest United States and over land areas worldwide under twentieth-century climate change (Croke et al. 1999; Karl et al. 1993).

Such changes in low-level cloudiness would have a profound effect on the surface warming under climate change. Increased cloudiness reduces the incident solar radiation at the surface, producing a cooling effect during daylight hours. The increased cloudiness also increases downwelling infrared radiation, which produces a warming effect throughout the diurnal cycle. The net result is a decrease in the diurnal range. Additionally, there is substantial snow loss in the spring, increasing shortwave absorption at the surface. When averaged over all times, the net radiation at the surface shows a slight decrease in the coastal lowlands, moderating the warming relative to the global model. Over the remainder of the region, the combined effects of decreased albedo and increased downwelling longwave radiation amplify the warming relative to the global model.

6. Regional effects on precipitation

The consensus among climate model simulations performed for the IPCC AR4 indicates a modest increase in precipitation over the Pacific Northwest during the months from November through January (Christensen et al. 2007; Salathé 2006), with increases of about 10%–15% for 2050–2100 relative to 1950–99, with approximately half of this enhancement in November. The increase appears to be related to changes in the midlatitude storm tracks, which move poleward and intensify under climate change (Yin 2005). At the regional scale, simulations of precipitation over Europe using regional climate models with approximately 50-km resolution (Frei et al. 1998; Frei et al. 2003) show increased precipitation in the winter season. In an earlier study of regional climate simulations for the Pacific Northwest using a 90-km-resolution model, Leung and Ghan (1999) showed a considerable enhancement of precipitation over the region. Snyder et al. (2002), using a regional model forced by a simulation using the NCAR Community Climate Model version 3 (CCM3), found large increases in precipitation over northern California under a $2 \times CO_2$ experiment. These prior studies suggest that there are two influences on precipitation under climate change—the first is related to changes in the large-scale moisture flux and storm patterns, which can be resolved by global modes, and the second relates to mesoscale interactions with the surface orography, which can only be captured in a high-resolution model.

Not all climate models simulate an increase in precipitation, and regional simulations tend to follow the response of the driving model. In simulations using a MM5-based regional climate model with 50-km grid spacing and forced by an ensemble of three Parallel Climate Model (PCM) simulations, Leung et al. (2004) found no statistically significant change in precipitation resulting from climate change over the western United States. However, compared to a large sample of global models (Salathé et al. 2007), the PCM produces a relatively small precipitation response, the ECHAM5 yields a moderate increase, and some models produce a considerably larger response than that of ECHAM5.

The regional patterns of precipitation change are considerably different from the global simulation. Here we will discuss the pattern for SON in the 2045–54 regional simulation, which shows a large increase in precipitation along the full length of the Cascade Range (Fig. 15c). The mechanisms producing changes in regional-scale precipitation are suggested by statistical downscaling results using two empirical methods (Salathé 2005; Widmann et al. 2003). In both methods, 1/8° gridded observed precipitation (Maurer et al. 2002; Widmann and Bretherton 2000) is used to develop a scaling factor at 1/8° resolution. The scaling factor is tuned during the 50-yr training period of 1950–99, where the observations and historic global simulation overlap. Precipitation simulated by the climate model is

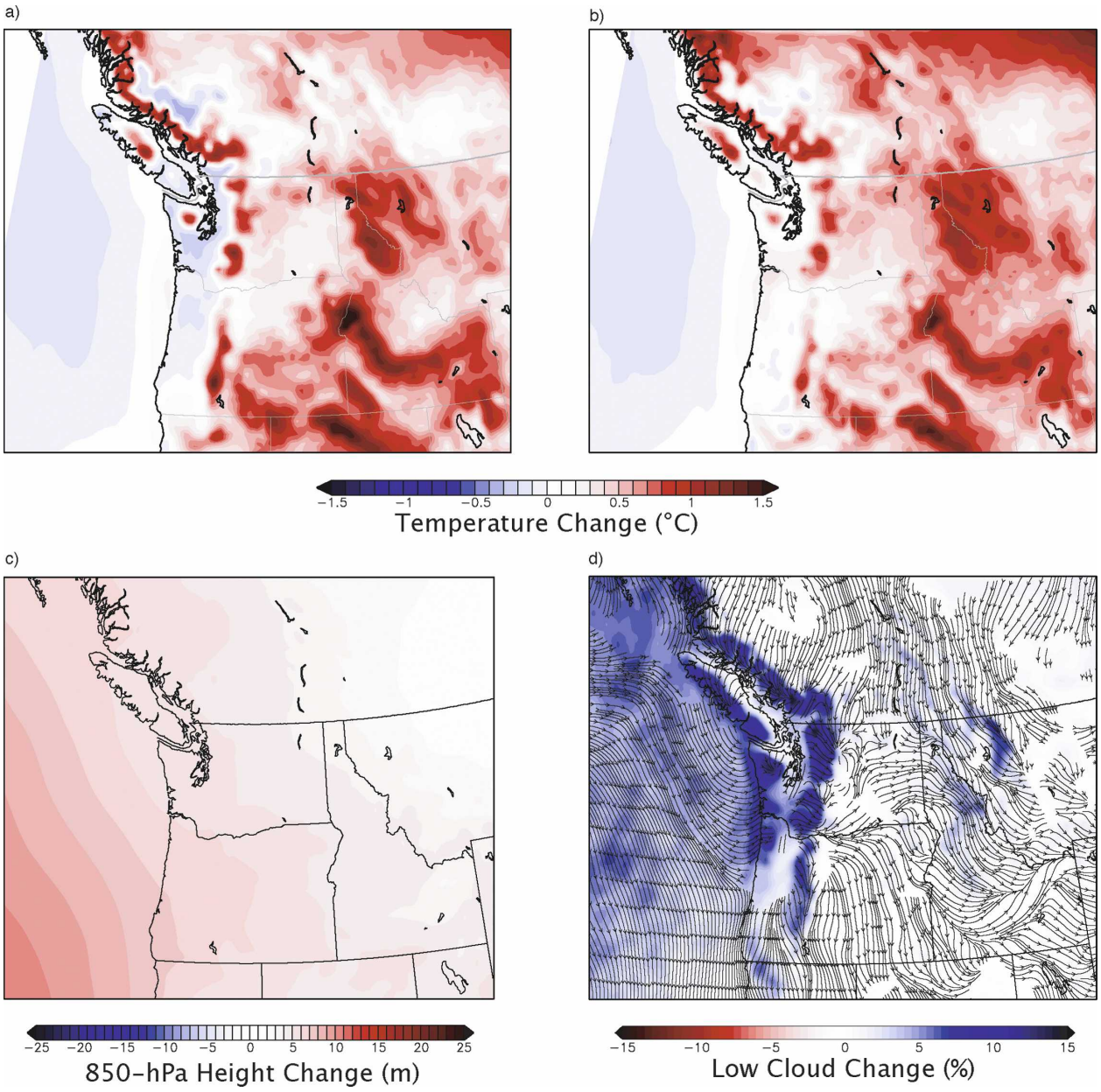

FIG. 14. Changes from 1990s to 2050s March–May season for difference in raw model change and mesoscale model change in 2-m (a) Tmax and (b) Tmin (°C). Positive values indicate larger warming in the regional simulation. Simulated MAM changes from 1989–99 to 2045–54 for (c) 850-hPa heights (m) and (d) integrated cloud water (ppmv) and surface wind.

sampled onto the 1/8° grid and the product between this and the empirical scaling factor yields the downscaled precipitation field. In the first method, only the global model precipitation is used to develop the scaling. In the second method, both global model precipitation and sea level pressure are used, and the scaling factor is fit during the training period to maintain the observed covariance between sea level pressure and precipitation. The large-scale circulation patterns over the Pacific Northwest control the orographic enhancement of precipitation on the upwind slopes of the Cascade and Coast Ranges and the rain shadow in eastern Washington and Oregon. Thus, the first method indicates the changes in regional precipitation that are captured only by the precipitation field in the model. This result would capture effects resulting from, for example, changes in the large-scale moisture flux and changes in the frequency and intensity of large-scale storms. The

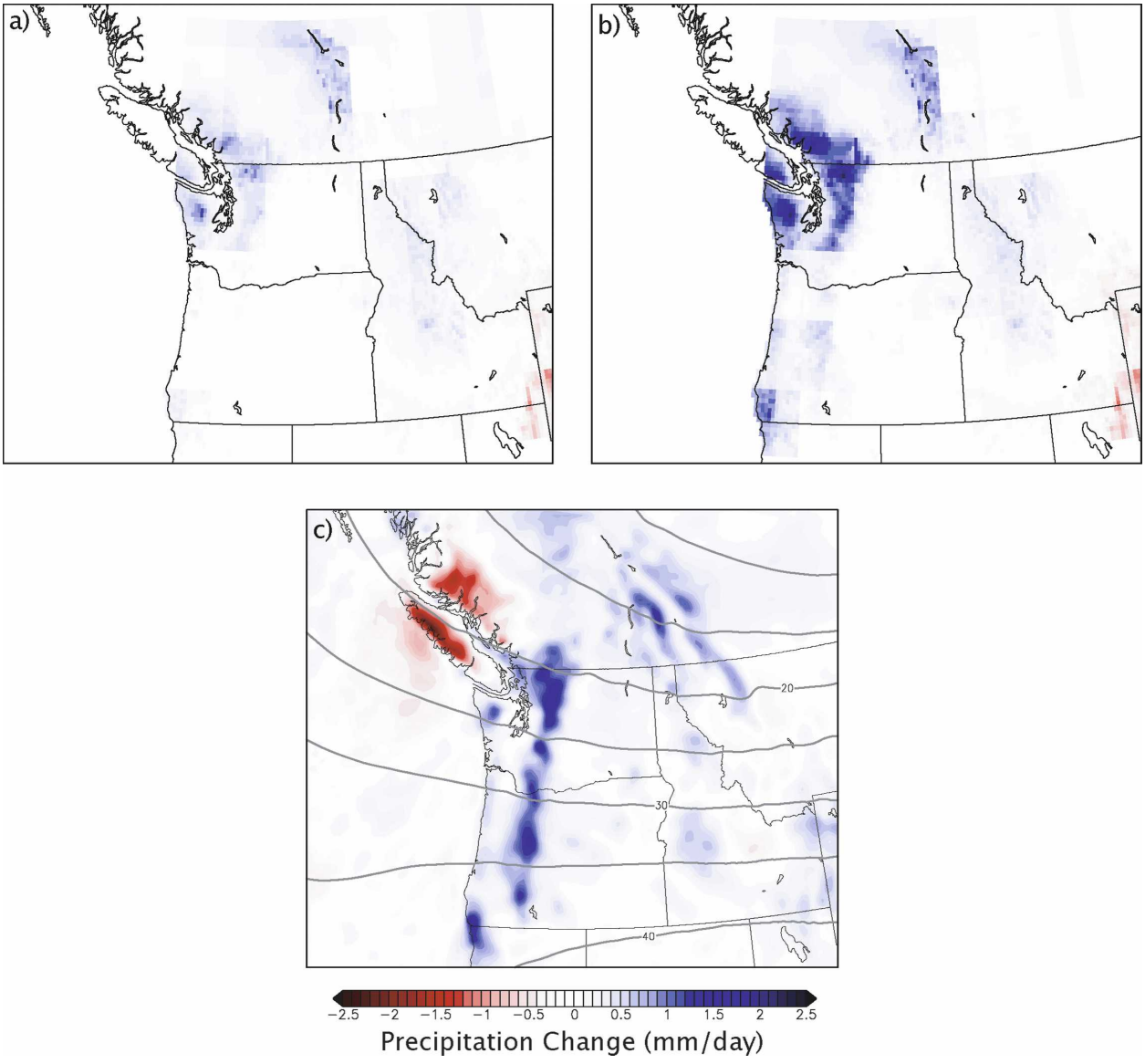

FIG. 15. Change in precipitation (mm day^{-1}) for SON season from 1989–99 to 2045–54 for (a) downscaling with precipitation only, (b) downscaling with precipitation and sea level pressure, and (c) regional model [contour lines: change in 500-hPa height (m)].

second method includes additional perturbations in regional precipitation caused by changes in the large-scale circulation, which helps account for interactions with the regional topography.

Figure 15a shows the change in precipitation from 1990–99 to 2045–54 from the precipitation-only downscaling (the statistical downscaling does not extend over Vancouver Island and western British Columbia). The result in Fig. 15a is the same sign as the change from ECHAM5 everywhere, but the magnitude is scaled in relation to the magnitude of the observed precipitation. With this downscaling applied, the ECHAM5 model predicts modest changes in precipitation over the northern portion of the domain. The second downscaling method indicates a considerably greater precipitation increase that extends farther south along the Cascade Range (Fig. 15b), indicating an orographic enhancement associated with the changes in atmospheric circulation. The second downscaling method attempts to relate circulation changes with the regional distribution of precipitation in the present climate. Thus, the large-scale state in the climate change simulation is similar to the large-scale state during times of orographic enhancement in the present climate.

The ECHAM5–MM5 simulation (Fig. 15c) shows increases in precipitation that are generally similar to the second downscaling method (i.e., including the effects of circulation). Contour lines indicate the change in 500-hPa heights, showing a shift in the large-scale circulation to a more onshore flow. The magnitude of the precipitation increase in the ECHAM5–MM5 simulation is similar to the result for statistical downscaling (Fig. 15b), but the region of increased precipitation extends farther south along the full Cascade Range into Oregon. Similar increases are also seen for the Olympic Mountains and the coastal mountains of southern Oregon and northern California. To the north, there is a decrease over Vancouver Island and the British Columbia Coast Range. These mountain ridges follow a southeast–northwest line as opposed to the north–south line of the ridges in Washington and Oregon. Thus, the circulation shift from the southwest to westerly, which enhances the orographic effect over the north–south ridges in Washington and Oregon, would have the opposite effect for the northwest–southeast British Columbia ridges. Using observations and MM5 simulations, Leung et al. (2003) have shown that the southwesterly flow associated with El Niño reduce the orographic precipitation along the north–south Cascade Range, despite the increased moisture flux associated with southwesterly flow. In contrast, east of the Cascade Range, rainfall increases during El Niño. The results above suggest that similar interactions between orography and the large-scale flow will also be important under climate change. Statistical downscaling methods may be able to capture some of these effects. However, because the range of conditions simulated in future climate scenarios may not be fully represented by the historic record, and because orographic precipitation involves dynamic and thermodynamic processes at very small scales, a regional climate model is a more appropriate tool for capturing these interactions.

7. Conclusions

We have used high-resolution (15 km) simulations from the MM5 forced by the ECHAM5 global model to explore several mesoscale processes that modify climate change at the local level. In winter and spring, the snow–albedo effect acts at fine spatial scales to enhance local warming, with considerable amplification of warming along the margins of the present-day snowpack. In spring, an increased onshore pressure gradient strengthens the onshore flow, which increases coastal cloudiness, reduces the daytime warming trend, and reduces the diurnal temperature range. During autumn, the ECHAM5 global model shows an increase in the large-scale precipitation as well as changes in the prevailing circulation patterns. The shift to more onshore flow increases the orographic precipitation along the north–south ridges of the Cascade Range and parts of the Rockies.

These results give strong evidence that the local response of temperature and precipitation to climate change is influenced by finescale processes that are not captured by coarse-resolution global models. While this study is limited to a single scenario from a single global model, these fundamental results depend on physical mechanisms that appear to be robust. In particular, snow–albedo feedback enhances warming over regions in which snowpack is lost. We have confidence in the ability of the regional model used here to represent this effect, because it duplicated similar changes that are observed in the annual transition from January to April, when snow–albedo plays an important role in the seasonal cycle. Because the global model does not represent the local topography well, it cannot properly simulate snow–albedo feedback, which leads to areas where the coarse-resolution global model either underestimates or overestimates the warming rate. Warming in mountainous areas is critical to the impacts of climate change on the region because of the importance of the snowpack for regional water resources and ecology. Many areas in the Cascade Range show much greater rates of winter and spring warming in the regional model compared to the global model. These areas contain watersheds that supply municipal water and hydroelectric power to urban areas of Washington and Oregon. Increased winter warming would hasten the loss of snowpack that is essential for storing winter precipitation for summer consumption. On the other hand, reduced wintertime warming rates simulated by the regional model for the Canadian Rockies would suggest a lesser impact of climate change on the Columbia River, which is a critical source of power and water throughout the western United States. However, because the regional model shows greater warming over much of the Columbia River basin, in particular for the Snake River, a major tributary, the net effects on Columbia flows cannot be estimated from these results and further research using hydrologic simulations will be required.

For spring, the regional simulations show increased onshore flow and cloud cover. These changes considerably reduce the daytime warming rate relative to the global model, reducing the diurnal range. The reduced warming rate and decrease in solar radiance could have important impacts on air quality and consumptive water use for irrigation (both agricultural and landscape).

The magnitude of this effect depends on the cloud representation in the model. Blocking by coastal mountain ranges and associated mesoscale effects modulates this mechanism, and thus it cannot be represented in coarse-resolution models.

The response of regional precipitation to climate change is a complex interaction between large-scale storm systems, which are well resolved by global models, and the local terrain, which is not well resolved. Global model consensus of the Pacific Northwest climate change indicates an increase in autumn precipitation (Salathé 2006) and changes in the circulation associated with midlatitude storm tacks (Salathé 2006; Yin 2005). Statistical downscaling indicates that the simulated circulation changes should enhance precipitation along the north–south ridges of the Pacific Northwest, but such methods may miss significant features. In fact, the regional model suggests a more widespread increase in precipitation along the Cascade Range extending farther south than that indicated by statistical downscaling. Thus, while there is considerable interannual variability in these processes, there is strong evidence that the large-scale circulation patterns will be altered under climate change and that these changes will in turn modify orographic precipitation.

An outstanding question not addressed in this study is the statistical significance of the climate change patterns we have presented. To address these issues, longer simulations are required to better capture the interannual variability and to help separate long-term trends from variability. Furthermore, some of the results depend on particular aspects of the global model simulation and may not be seen in simulations forced by other global models. For example, the changes in precipitation and cloudiness are clearly related to large-scale circulation changes simulated by the ECHAM5 model. Similar changes are seen in other models, but with important differences that may influence the regional climate simulation. In future work, we will be extending this analysis to longer simulations and simulations with various forcing models.

Acknowledgments. This publication is funded by the Center for Science in the Earth System (CSES) and Joint Institute for the Study of the Atmosphere and Ocean (JISAO) under NOAA Cooperative Agreement NA17RJ1232, by National Science Foundation Grant 0709856, by an EPA STAR Grant, and by Seattle City Light. ECHAM5 model output was obtained from the CERA (online at http://cera-www.dkrz.de/CERA/index.html); the data are managed by the World Data Center of Climate (online at http://www.mad.zmaw.de/wdcc/).

APPENDIX

Parameterization for Deep Soil Temperature

Observations (Baxter 1997) and models (Jury et al. 1991) of soil temperature show that, at a depth of 3 m (lower soil boundary in the Noah LSM), the annual soil temperature cycle is typically time lagged by 70 days and amplitude damped to about one-third the amplitude of the skin temperature. For climate simulations over many years, a fixed climatological boundary condition would force errors in the surface parameters. Therefore, we have implemented a parameterization to update the 3-m lower boundary soil temperature based on simulated skin temperature. The phase lag and attenuation at depth depend on the frequency of the surface temperature variation, but we shall base our methodology on the annual cycle. The desired response may be obtained by taking a simple weighted average of the skin temperature over the previous year, where the weighting is adjusted to yield the desired attenuation and phase lag. We choose a weighting function with two terms, the skin temperature averaged over the past year $\langle T_{\text{skin}}\rangle_{365}$ and the past n days prior to the time of interest $\langle T_{\text{skin}}\rangle_{n}$,

$$T_{\text{soil}} = \alpha\langle T_{\text{skin}}\rangle_{365} + (1 - \alpha)\langle T_{\text{skin}}\rangle_{n}, \qquad \text{(A1)}$$

where α and n are a function of depth and tuned to produce the desired attenuation and phase lag for the depth of interest. For 3-m depth, we use the published observed values of 30% attenuation and 70-days lag (Baxter 1997) to obtain $\alpha = 0.6$ and $n = 140$ days.

Because good observations of soil temperatures at a 3-m depth are not readily available, to test this method we used surface and 1.78-m-deep soil temperatures observed at Ames, Iowa (Jackson 2003). For 1.78-m depth, we use $\alpha = 0.3$ and $n = 46$ days to obtain the observed lag and attenuation. In Fig. A1, the solid line shows the observed 1.78-m soil temperature and the dashed line is skin temperature with a 46-day running mean applied. The weighted mean of the skin temperature yields the dotted line, which closely captures the form of the observed 1.78-m soil temperature over four seasonal cycles.

When applied to the MM5 climate modeling system, this soil temperature parameterization uses surface skin temperatures generated by MM5 and the Noah LSM to derive the 3-m soil temperature. For the first year of each decade-long simulation, however, previous MM5 output is not available, and must be derived from a spinup simulation (i.e., a preliminary simulation not used in the analysis of results, but only to spin up model parameters) using skin temperature from the forcing

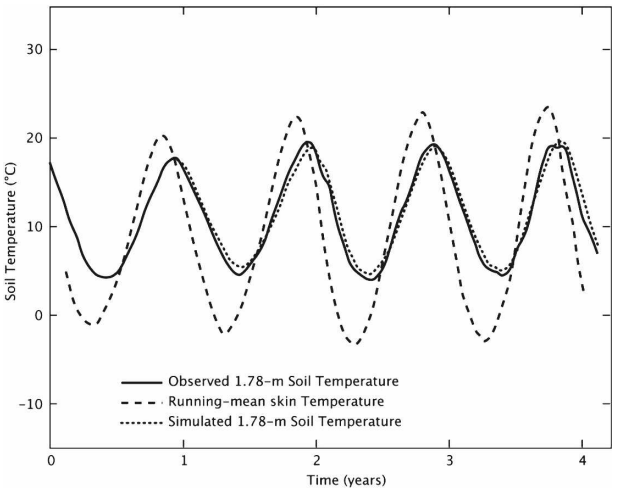

FIG. A1. Soil temperature observations and deep soil temperature estimation using parameterization described in text.

model. This spin up is also required to bring the Noah LSM soil temperature and moisture fields for the entire soil column into equilibrium with the simulated atmospheric state.

Studies (e.g., Cosgrove et al. 2003) have shown that, especially in drier regions, a spinup period of at least a year is necessary for soil moisture, because the land surface model slowly adjusts soil parameters away from initial values. Thus, the spinup simulations are initialized at the end of summer (September 1989), when soils are climatologically driest in the Pacific Northwest. For simplicity, we use the same forcing data for the spinup as for the first year of the actual climate simulation. At initialization, the global forcing model (i.e., either NNRP or ECHAM5) is used in Eq. (A1) to compute the lower boundary (3 m) soil temperature. Initial soil temperatures for all intervening layers (between the surface 3 m) in the Noah LSM are linearly interpolated and then allowed to evolve according to the LSM throughout the simulation. Soil moisture is initialized with the climatological values provided in MM5 and then allowed to evolve over the spinup year according to the LSM. As MM5 surface data became available at each time step, the parameterization was updated at each grid point using the available MM5 output, thereby phasing out the coarse global model data and allowing mesoscale variations in the soil parameters. The deep soil temperature parameterization was implemented with a 6-hourly time step. At the completion of the spinup year, a complete year of MM5-derived skin temperatures is available for the deep soil parameterization and the soil temperature and moisture profile has spun up to the atmospheric forcing.

REFERENCES

Achberger, C., M. L. Linderson, and D. Chen, 2003: Performance of the Rossby Centre regional atmospheric model in southern Sweden: Comparison of simulated and observed precipitation. *Theor. Appl. Climatol.,* **76,** 219–234.

Baxter, D. O., 1997: A comparison of deep soil temperature: Tennessee versus other locations. *Trans. ASAE,* **40,** 727–738.

Christensen, J. H., and P. Kuhry, 2000: High-resolution regional climate model validation and permafrost simulation for the East European Russian Arctic. *J. Geophys. Res.,* **105,** 29 647–29 658.

——, and Coauthors, 2007: Regional climate projections. *Climate Change 2007: The Physical Science Basis,* S. Solomon et al., Eds., Cambridge University Press, 847–940.

Colle, B. A., K. J. Westrick, and C. F. Mass, 1999: Evaluation of MM5 and Eta-10 precipitation forecasts over the Pacific Northwest during the cool season. *Wea. Forecasting,* **14,** 137–154.

——, C. F. Mass, and K. J. Westrick, 2000: MM5 precipitation verification over the Pacific Northwest during the 1997–99 cool seasons. *Wea. Forecasting,* **15,** 730–744.

Cosgrove, B. A., and Coauthors, 2003: Land surface model spinup behavior in the North American Land Data Assimilation System (NLDAS). *J. Geophys. Res.,* **108,** 8845, doi:10.1029/2002JD003316.

Croke, M. S., R. D. Cess, and S. Hameed, 1999: Regional cloud cover change associated with global climate change: Case studies for three regions of the United States. *J. Climate,* **12,** 2128–2134.

Dudhia, J., 1989: Numerical study of convection observed during the Winter Monsoon Experiment using a mesoscale two-dimensional model. *J. Atmos. Sci.,* **46,** 3077–3107.

Duffy, P. B., B. Govindasamy, J. P. Iorio, J. Milovich, K. R. Sperber, K. E. Taylor, M. F. Wehner, and S. L. Thompson, 2003: High-resolution simulations of global climate, Part 1: Present climate. *Climate Dyn.,* **21,** 371–390.

——, and Coauthors, 2006: Simulations of present and future climates in the western United States with four nested regional climate models. *J. Climate,* **19,** 873–895.

Frei, C., C. Schär, D. Lüthi, and H. C. Davies, 1998: Heavy precipitation processes in a warmer climate. *Geophys. Res. Lett.,* **25,** 1431–1434.

——, J. H. Christensen, M. Déqué, D. Jacob, R. G. Jones, and P. L. Vidale, 2003: Daily precipitation statistics in regional climate models: Evaluation and intercomparison for the European Alps. *J. Geophys. Res.,* **108,** 4124, doi:10.1029/2002JD002287.

Giorgi, F., and L. O. Mearns, 1999: Introduction to special section: Regional climate modeling revisited. *J. Geophys. Res.,* **104,** 6335–6352.

——, J. W. Hurrell, M. R. Marinucci, and M. Beniston, 1997: Elevation dependency of the surface climate change signal: A model study. *J. Climate,* **10,** 288–296.

Grell, G., J. Dudhia, and D. R. Stauffer, 1993: A description of the fifth generation Penn State/NCAR mesoscale model (MM5). NCAR Tech. Note NCAR/TN-398+IA, 107 pp.

Hack, J. J., B. A. Boville, J. P. Briegleb, J. T. Kiehl, P. J. Rasch, and D. L. Williamson, 1993: Description of the NCAR Community Climate Model (CCM2). NCAR Tech. Note NCAR/TN-883+STR, 108 pp.

Holland, M. M., and C. M. Bitz, 2003: Polar amplification of climate change in coupled models. *Climate Dyn.,* **21,** 221–232.

Hong, S. Y., and H. L. Pan, 1996: Nonlocal boundary layer vertical diffusion in a Medium-Range Forecast Model. *Mon. Wea. Rev.,* **124,** 2322–2339.

Jackson, T. J., 2003: SMEX02 Soil Climate Analysis Network (SCAN) station 2031, Ames, Iowa. National Snow and Ice Data Center, Boulder, CO, digital media. [Available online at http://nsidc.org/data/docs/daac/nsidc0142_smex_scan.gd.html.]

Jury, W. A., W. R. Gardner, and W. H. Gardner, 1991: *Soil Physics.* 5th ed. Wiley and Sons, 328 pp.

Kain, J. S., and J. M. Fritsch, 1993: Convective parameterization for mesoscale models: The Kain–Fritsch scheme. *The Representation of Cumulus Convection in Numerical Models, Meteor. Monogr.,* No. 46, Amer. Meteor. Soc., 165–170.

Kalnay, E., and Coauthors, 1996: The NCEP/NCAR 40-Year Reanalysis Project. *Bull. Amer. Meteor. Soc.,* **77,** 437–471.

Karl, T. R., J. C. N. Williams, F. T. Quinlan, and T. A. Boden, 1990: United States Historical Climatology Network (HCN) serial temperature and precipitation data. Carbon Dioxide Information and Analysis Center, Oak Ridge National Laboratory, Environmental Science Division Publication 3404, 389 pp.

——, and Coauthors, 1993: A new perspective on recent global warming: Asymmetric trends of daily maximum and minimum temperature. *Bull. Amer. Meteor. Soc.,* **74,** 1007–1023.

Leung, L. R., and S. J. Ghan, 1999: Pacific Northwest climate sensitivity simulated by a regional climate model driven by a GCM. Part II: 2 × CO_2 simulations. *J. Climate,* **12,** 2031–2053.

——, and Y. Qian, 2003: The sensitivity of precipitation and snowpack simulations to model resolution via nesting in regions of complex terrain. *J. Hydrometeor.,* **4,** 1025–1043.

——, ——, X. Bian, and A. Hunt, 2003: Hydroclimate of the western United States based on observations and regional climate simulation of 1981–2000. Part II: Mesoscale ENSO anomalies. *J. Climate,* **16,** 1912–1928.

——, ——, ——, W. M. Washington, J. Han, and J. O. Roads, 2004: Mid-century ensemble regional climate change scenarios for the western United States. *Climatic Change,* **62,** 75–113.

Marsland, S. J., H. Haak, J. H. Jungclaus, M. Latif, and F. Roske, 2003: The Max-Planck-Institute global ocean/sea ice model with orthogonal curvilinear coordinates. *Ocean Modell.,* **5,** 91–127.

Mass, C. F., and Y.-H. Kuo, 1998: Regional real-time numerical weather prediction: Current status and future potential. *Bull. Amer. Meteor. Soc.,* **79,** 253–263.

——, D. Ovens, K. Westrick, and B. A. Colle, 2002: Does increasing horizontal resolution produce more skillful forecasts? *Bull. Amer. Meteor. Soc.,* **83,** 407–430.

——, and Coauthors, 2003: Regional environmental prediction over the Pacific Northwest. *Bull. Amer. Meteor. Soc.,* **84,** 1353–1366.

Maurer, E. P., A. W. Wood, J. C. Adam, D. P. Lettenmaier, and B. Nijssen, 2002: A long-term hydrologically based dataset of land surface fluxes and states for the conterminous United States. *J. Climate,* **15,** 3237–3251.

Nakicenovic, N., and R. Swart, Eds., 2000: *Emissions Scenarios*. Cambridge University Press, 599 pp.

Roeckner, E., L. Bengtsson, J. Feichter, J. Lelieveld, and H. Rodhe, 1999: Transient climate change simulations with a coupled atmosphere–ocean GCM including the tropospheric sulfur cycle. *J. Climate,* **12,** 3004–3032.

——, and Coauthors, 2003: The atmospheric general circulation model ECHAM5, Part I: Model description. Max-Planck-Institute for Meteorology Rep. 349, 140 pp.

Salathé, E. P., Jr., 2003: Comparison of various precipitation downscaling methods for the simulation of streamflow in a rain shadow river basin. *Int. J. Climatol.,* **23,** 887–901.

——, 2005: Downscaling simulations of future global climate with application to hydrologic modeling. *Int. J. Climatol.,* **25,** 419–436.

——, 2006: Influences of a shift in North Pacific storm tracks on western North American precipitation under global warming. *Geophys. Res. Lett.,* **33,** L19820, doi:10.1029/2006GL026882.

——, P. W. Mote, and M. W. Wiley, 2007: Review of scenario selection and downscaling methods for the assessment of climate change impacts on hydrology in the United States Pacific northwest. *Int. J. Climatol.,* **27,** 1611–1621.

Snyder, M. A., J. L. Bell, L. C. Sloan, P. B. Duffy, and B. Govindasamy, 2002: Climate responses to a doubling of atmospheric carbon dioxide for a climatically vulnerable region. *Geophys. Res. Lett.,* **29,** 1514, doi:10.1029/2001GL014431.

Tebaldi, C., K. Hayhoe, J. M. Arblaster, and G. A. Meehl, 2006: Going to the extremes. *Climatic Change,* **79,** 185–211.

von Storch, H., H. Langenberg, and F. Feser, 2000: A spectral nudging technique for dynamical downscaling purposes. *Mon. Wea. Rev.,* **128,** 3664–3673.

Wang, Y. Q., L. R. Leung, J. L. McGregor, D. K. Lee, W. C. Wang, Y. H. Ding, and F. Kimura, 2004: Regional climate modeling: Progress, challenges, and prospects. *J. Meteor. Soc. Japan,* **82,** 1599–1628.

Widmann, M., and C. S. Bretherton, 2000: Validation of mesoscale precipitation in the NCEP reanalysis using a new grid-cell dataset for the northwestern United States. *J. Climate,* **13,** 1936–1950.

——, ——, and E. P. Salathé, 2003: Statistical precipitation downscaling over the northwestern United States using numerically simulated precipitation as a predictor. *J. Climate,* **16,** 799–816.

Wood, A. W., L. R. Leung, V. Sridhar, and D. P. Lettenmaier, 2004: Hydrologic implications of dynamical and statistical approaches to downscaling climate model outputs. *Climatic Change,* **62,** 189–216.

Yin, J. H., 2005: A consistent poleward shift of the storm tracks in simulations of 21st century climate. *Geophys. Res. Lett.,* **32,** L18701, doi:10.1029/2005GL023684.